Quantifying Changes in Future Intensity-Duration-Frequency Curves Using Multimodel Ensemble Simulations

Elisa Ragno[1] ![ID], Amir AghaKouchak[1] ![ID], Charlotte A. Love[1] ![ID], Linyin Cheng[2] ![ID], Farshid Vahedifard[3] ![ID], and Carlos H. R. Lima[4] ![ID]

[1]Department of Civil and Environmental Engineering, University of California, Irvine, California, USA, [2]Cooperative Institute for Research in Environmental Sciences, University of Colorado, Boulder, Colorado, USA, [3]Department of Civil and Environmental Engineering, Mississippi State University, Mississippi, USA, [4]Civil and Environmental Engineering, University of Brasilia, Brasilia, Brazil

Abstract During the last century, we have observed a warming climate with more intense precipitation extremes in some regions, likely due to increases in the atmosphere's water holding capacity. Traditionally, infrastructure design and rainfall-triggered landslide models rely on the notion of stationarity, which assumes that the statistics of extremes do not change significantly over time. However, in a warming climate, infrastructures and natural slopes will likely face more severe climatic conditions, with potential human and socioeconomical consequences. Here we outline a framework for quantifying climate change impacts based on the magnitude and frequency of extreme rainfall events using bias corrected historical and multimodel projected precipitation extremes. The approach evaluates changes in rainfall Intensity-Duration-Frequency (IDF) curves and their uncertainty bounds using a nonstationary model based on Bayesian inference. We show that highly populated areas across the United States may experience extreme precipitation events up to 20% more intense and twice as frequent, relative to historical records, despite the expectation of unchanged annual mean precipitation. Since IDF curves are widely used for infrastructure design and risk assessment, the proposed framework offers an avenue for assessing resilience of infrastructure and landslide hazard in a warming climate.

1. Introduction

The Fifth Assessment Report of the Intergovernmental Panel on Climate Change (IPCC; Pachauri et al., 2014) states that since 1960 anthropogenic activities have likely contributed to altering the global water cycle by increasing, more than decreasing, the number of heavy precipitation events in terrestrial regions. Indeed, higher surface temperatures observed over the past decades (e.g., Barnett et al., 1999; Diffenbaugh et al., 2015; Fischer & Knutti, 2015; Mazdiyasni & AghaKouchak, 2015; Melillo et al., 2014), mainly driven by human activities (Melillo et al., 2014; Stott et al., 2010; Zhang et al., 2006; Zwiers et al., 2011), can alter the hydrological cycle leading to more intense rainfall events (Cheng et al., 2014; Fischer & Knutti, 2016; Marvel & Bonfils, 2013; Min et al., 2011; Westra et al., 2013; Zhang et al., 2007). Reports indicate that many regions including the United States, central Africa, parts of southwest Asia (i.e., Thailand, Taiwan), Central America, Australia, and parts of eastern Europe have experienced more extreme events (DeGaetano, 2009; Fischer & Knutti, 2015; Melillo et al., 2014; Wasko et al., 2016; Zheng et al., 2015). Heavier precipitation events have increased the risk of flooding at regional scale (Pachauri et al., 2014) and rainfall-triggered landslide activity in the United States over the past few decades (Gariano & Guzzetti, 2016). Moreover, recent studies using precipitation projections from Global Climate Models (GCMs) indicate that there is a high chance of substantial impact on landslide activity in natural slopes (Robinson et al., 2017) and on the performance of man-made earthen structures (Jasim et al., 2017; Vahedifard et al., 2017).

The observed trends and projected changes in future extreme events have called into question the preparedness of existing and future construction (Hallegatte et al., 2013; Mailhot & Duchesne, 2010; Milly et al., 2008; Moftakhari et al., 2017; Yan et al., 2018). Current design and failure risk assessment procedures for infrastructure (e.g., dams, roads, sewer, and storm water drainage systems) and earthen structures (e.g., levees, natural, and engineered slopes) rely on rainfall Intensity-Duration-Frequency (IDF) curves for estimating the design storm intensity and the corresponding flow. IDF curves represent the probable intensity of a

rainfall event given a certain duration (or time of concentration—e.g., 24 h) and an average return period (recurrence interval), estimation of which involves fitting a representative distribution function to observed precipitation (Bonnin et al., 2006). In the current procedure, the parameters of the distribution are estimated under the so-called stationary assumption (i.e., time-invariant parameters). This assumes that no significant changes are expected in magnitude or frequency, and hence in distribution parameters of precipitation extremes over time (Milly et al., 2008).

Several studies have considered nonstationary models for extreme value analysis to address temporal changes in climate extremes (Huard et al., 2009; Katz, 2013; Katz et al., 2002; Krishnaswamy et al., 2015; Lima et al., 2016; Mailhot et al., 2007; Mirhosseini et al., 2014, 2015; Mondal & Mujumdar, 2015; Obeysekera & Salas, 2013; Read & Vogel, 2015; Sadegh et al., 2015; Salas & Obeysekera, 2013; Sankarasubramanian & Lall, 2003; Sarhadi & Soulis, 2017; Villarini et al., 2010; Vogel et al., 2011; Volpi et al., 2015; Willems et al., 2012; Yil-maz & Perera, 2014; Zhu et al., 2012). Among those, Cooley et al. (2007) proposed a spatiotemporal Bayesian hierarchical modeling approach for defining IDF maps for flood management in the Front Range of Colorado. Villarini et al. (2009) presented a framework for dealing with annual maximum peak discharge under nonstationary conditions. Rosner et al. (2014) introduced a novel methodology for flood risk assessment integrating the concepts of under-preparedness and over-preparedness in a nonstationary context. Cheng et al. (2014) developed a Bayesian-based framework for analyzing time-dependent extremes. Reliable nonstationary analysis, however, requires understanding the deterministic process(es) causing time-variant behavior (Cohn & Lins, 2005; Koutsoyiannis, 2005; Koutsoyiannis & Montanari, 2015; Lins & Cohn, 2011; Montanari & Koutsoyiannis, 2014; Serinaldi & Kilsby, 2015). For this reason, projecting observed historical trends may lead to unreliable estimates of frequency for future extremes (Luke et al., 2017; Serinaldi & Kilsby, 2015).

One limitation of the methodologies proposed lies in the use of solely observed historical data for nonstationary extreme value analysis, with some assumption on future trends. However, Global Climate Models (GCM), although they exhibit high uncertainty, offer plausible scenarios of future climate and can be implemented for extreme value analysis, in particular for deriving future IDF curves. Therefore, we first outline a new methodology for deriving multimodel nonstationary IDF curves. It incorporates simulations from multiple GCMs processed using the nonstationary extreme value analysis method proposed by Cheng et al. (2014). The IDF curves derived will then include information from both climate intermodel variability and precipitation changes over time. We then introduce the concept of safety factor, i.e., ratio of medians of the future relative to the past IDF curves, for practitioners who want to account for future changes in infrastructure loads (i.e., precipitation) during the design process and risk analysis. We, finally, propose a new way of communicating the risk of hazardous climatic conditions by calculating the expected future return period (i.e., average occurrence of an event in years) of events which, based on historical observations, have a return period of 25, 50, and 100 years. Indeed, characterizing changes in extreme events in terms of changes in the associated return period can be more easily interpreted by both experts and nonexperts. We will apply the new framework to annual precipitation maxima intensity in a number of urban areas across the United States to calculate updated future IDF curves, expected future changes in the frequency (return period) of extreme precipitation intensity, and safety factors for the locations investigated.

2. Data

In this study, we focus on extreme precipitation events in a number of cities across the United States (see supporting information Tables S2 and S3), where urbanization, when compounded with rare precipitation events, can lead to extreme floods and landslide activity with potentially high impacts on the population.

We retrieved downscaled GCM simulations of historical and projected precipitation from the Coupled Model Intercomparison Project Phase 5 (CMIP5), made available through the online archive Downscaled CMIP3 and CMIP5 Climate and Hydrology Projections (DCHP; Brekke et al., 2013). Future projections are based on four Representative Concentration Pathways (RCPs) each of them describing a potential future GHG concentration trajectory during the twenty-first century (IPCC2014; Pachauri et al., 2014).

For this study, we selected the CMIP5-BCCAv2 (Bias Corrected Constructed Analogs) daily precipitation products with 1/8° spatial resolution, developed using the constructed analogs downscaling method, and bias corrected based on available observations, using a quantile mapping technique (Hidalgo et al., 2008).

We selected the models in supporting information Table S1 that provide the following simulations: historical simulations from 1950 to 1999, and future projections between 2050 and 2099 from RCP4.5 (moderate GHG concentration trajectory) and RCP8.5 (very high GHG concentration trajectory). The interval selected for our historical simulations (1950–1999) coincides with the period of time in which the historical simulations were adjusted based on available observations (Hidalgo et al., 2008).

Afterward, we processed GCM daily precipitation to obtain time series of annual maxima precipitation intensity within a water year (October–September, as defined by the United States Geological Survey—USGS) for events of 1–7 days duration. The duration of precipitation events in the present study (1 day events and higher) has been constrained by the time resolution of the GCM simulations. A time series of annual maxima is retrieved as follows. Let us consider the time series of daily precipitation of the j'th water year, $P^j = \{p_1^j, \ldots, p_{n_j}^j\}$, where n_j is the number of days in the j'th water year. The annual maximum precipitation intensity of a d day event for the j'th water year is $P_{d,\max}^j = \max \left\{ \frac{\sum_{t=1}^{d} p_t^j}{d}, \ldots, \frac{\sum_{t=i}^{i+d-1} p_t^j}{d}, \ldots, \frac{\sum_{t=n_j-d+1}^{n_j} p_t^j}{d} \right\}$. The time series of annual maxima is then $P_{d,\max} = \{P_{d,\max}^1, \ldots, P_{d,\max}^{ny}\}$, where ny is the total number of water years. We processed the historical simulations and the projections independently, model by model. Each time series consists of 49 water years (number of water years contained in a 50 year period). Thus, each station has the following set of time series: $HE_{m,d}^s$, $FE45_{m,d}^s$, and $FE85_{m,d}^s$ corresponding to historical simulations, RCP4.5, and RCP8.5 projections, respectively; s indicates the urban area; m refers to the GCM; d expresses the duration of the event in days.

3. Methodology

3.1. Distance Components Test

Here we are interested in characterizing changes in historical and future precipitation simulations. Specifically, we are interested in testing the null-hypothesis of equal distributions and equal means between extreme precipitation from historical and future simulations to assess whether the statistics of extremes are expected to change. There are specific tests for assessing equal distributions (e.g., Kolmogorov-Smirnov test (Massey, 1951), Cramér-von Mises test (Anderson, 1962), Anderson-Darling test (Anderson, 2011)), equal means (e.g., analysis of variance (ANOVA) test, Student's t test), presence of a monotonic trend (e.g., Mann-Kendall trend test (Mann, 1945)). Here we have adopted the Distance Components (DISCO) test proposed by Rizzo and Székely (2010) that combines equal distribution and equal mean tests. This method is a nonparametric extension of the analysis of variance (ANOVA) and the multivariate analysis of variance (MANOVA) tests as a more generalized hypothesis testing framework (Rizzo & Székely, 2010; Székely & Rizzo, 2013). Compared to the classical ANOVA and MANOVA tests, the DISCO test does not require a minimum sample size and/or homogeneity of the error variance (Rizzo & Székely, 2010), and it can be implemented under different null-hypotheses (i.e., equal means and equal distributions) eliminating the need for additional tests. Moreover, the test, available in the R package *energy*, is performed by permutation, avoiding any dependence on the choice of the distribution (Rizzo & Székely, 2010; Székely & Rizzo, 2013).

The DISCO test is derived as follows. A version of the Gini mean distance statistic between two samples $A = \{a_1, \ldots, a_{n_1}\}$ and $B = \{b_1, \ldots, b_{n_1}\}$ is defined as follows (Rizzo & Székely, 2010):

$$g_\alpha(A, B) = \frac{1}{n_1 \cdot n_2} \cdot \sum_{i=1}^{n_1} \sum_{j=1}^{n_2} ||a_i - b_j||^\alpha = E[||A - B||^\alpha] \tag{1}$$

where $|| \cdot ||$ is the Euclidean norm, and $0 < \alpha \leq 2$.

Let us consider K samples $X_1, \ldots, X_K$ of sizes $n_1, \ldots, n_K$. Analogous to the decomposition of the variance in the ANOVA test, the total dispersion of the K samples T_α is (Rizzo & Székely, 2010; Székely & Rizzo, 2013):

$$T_\alpha = T_\alpha(X_1, \ldots, X_K) = \frac{N}{2} \cdot g_\alpha(X, X) \tag{2}$$

where $N = \sum_{k=1}^{K} n_k$ and X is the pooled sample. Moreover, the within-sample dispersion, W_α, and the between-sample dispersion, S_α, are (Rizzo & Székely, 2010; Székely & Rizzo, 2013):

$$W_\alpha = W_\alpha(X_1, \ldots, X_K) = \sum_{k=1}^{K} \frac{n_k}{2} \cdot g_\alpha(X_k, X_k) \tag{3}$$

$$S_\alpha = S_\alpha(X_1, \ldots, X_K) = \sum_{1 \leq j < k \leq K} \left[\frac{n_j + n_k}{2N} \right] \cdot \left[\frac{n_j \cdot n_k}{n_j + n_k} \cdot \varepsilon_\alpha(X_j, X_k) \right] \tag{4}$$

where $\varepsilon_\alpha = (2g_\alpha(X_j, X_k) - g_\alpha(X_j, X_j) - g_\alpha(X_k, X_k))$ is the Energy distance (ε_α-distance). For $0 < \alpha \leq 2$, the decomposition $T_\alpha = W_\alpha + S_\alpha$ holds and W_α and S_α are nonnegative (Rizzo & Székely, 2010; Székely & Rizzo, 2013). For $K \geq 2$ and $0 < \alpha \leq 2$, and $X_1, \ldots, X_K$ independent and identically distributed (i.i.d.), the following statements about S_α hold:

1. $S_\alpha(X_1, \ldots, X_K) \geq 0$;
2. for $0 < \alpha < 2$, $S_\alpha(X_1, \ldots, X_K) = 0$ if and only if $X_1 = \cdots = X_K$;
3. $\alpha = 2$, $S_2(X_1, \ldots, X_K) = 0$, if and only if $X_1, \ldots, X_K$ have equal means.

For proof and details see Theorem 1 and Corollary 1 in Rizzo and Székely (2010).

Given the properties of S_α, Rizzo and Székely (2010) proposed the following statistic for testing equal distributions:

$$F_\alpha = \left(\frac{S_\alpha}{K-1} \right) \cdot \left(\frac{N-K}{W_\alpha} \right) \tag{5}$$

F_α does not have an F-distribution, but it is nonnegative and takes large values when the samples $X_1, \ldots, X_K$ are drawn from nonequal distribution, supporting the alternative hypothesis (Rizzo & Székely, 2010).

Here we implemented the test considering two values of the index α: $\alpha = 1$ to test the null-hypothesis of equal distributions between pairs of time series, and $\alpha = 2$ to test the null-hypothesis of equal means between pairs of time series. The former choice corresponds to the Euclidean distance and allows g_α (equation (1)) to be linearized, reducing the computational effort (Rizzo & Székely, 2010). The latter choice adds information about the mean of the two samples.

3.2. Extreme Value Analysis for IDF Curves

Precipitation-based IDF curves estimation involves fitting a representative distribution function to observed extreme precipitation (Bonnin et al., 2006). Extreme value analysis is widely used in hydrological design and risk assessment for a statistical representation of rare events (Coles, 2001). Time series of annual maxima are commonly described by the Generalized Extreme Value (GEV) distribution. The cumulative distribution function of the GEV distribution is (Cheng et al., 2014):

$$\Psi(x) = \exp \left\{ - \left(1 + \xi \cdot \left(\frac{x - \mu}{\sigma} \right) \right)^{-\frac{1}{\xi}} \right\} \tag{6}$$

for $\xi \cdot \left(\frac{x-\mu}{\sigma} \right) > 0$. μ, σ, and ξ are the statistics of the distribution: μ is the location parameter and represents the center of the distribution; σ is the scale parameter and describes the distribution of the data around μ; ξ is the shape parameter and defines the tail behavior of the distribution. Current IDF curves in the United States, available through the National Oceanic and Atmospheric Administration (NOAA), are derived based on the stationary GEV distribution (i.e., time independent parameters) shown in equation (6). The stationary GEV model can be adapted for time-dependent series by letting the parameters of the distribution be a function of time ($\mu(t)$, $\sigma(t)$, $\xi(t)$) (Coles, 2001), for a more realistic representation of the time series behavior (Cheng et al., 2014).

Here we derived future IDF curves of precipitation based on a GEV distribution with time-dependent statistics only upon detection of a statistically significant trend in the data (Mann-Kendall trend test (Mann, 1945) with a 0.05 level of significance). We used the nonstationary extreme value analysis (NEVA) framework proposed by Cheng et al. (2014) to estimate the distribution parameters because it has two main advantages:

1. It is versatile enough to deal with temporally stationary and nonstationary extremes (including annual maxima and extremes over a particular threshold).

2. It is based on Bayesian inference and Differential Evolution Markov Chain (DE-MC), which provide both parameter estimation and uncertainty quantification (Cheng et al., 2014).

Let θ be the parameter of a given distribution and let $\mathbf{Y} = \{y_1, \ldots, y_n\}$ be the set of n observations. Following the Bayes theorem, the probability of θ given $\mathbf{Y}$ (posterior) is proportional to the product of the probability of θ (prior) and the probability of $\mathbf{Y}$ given θ (likelihood function). Assuming independence between the observations $\mathbf{Y}$:

$$p(\theta|\mathbf{Y}) \propto \prod_{i=1}^{n} p(\theta) \cdot p(y_i|\theta) \tag{7}$$

In NEVA, the likelihood function is the GEV distribution, and θ is the vector containing the parameters of the GEV distribution to be estimated. In the stationary case, $\theta = \{\mu, \sigma, \xi\}$. Hence, considering independent GEV parameters:

$$p(\mu, \sigma, \xi|\mathbf{Y}) \propto \prod_{i=1}^{n} p(\mu) \cdot p(\sigma) \cdot p(\xi) \cdot p(y_i|\mu, \sigma, \xi) \tag{8}$$

In the case of a nonstationary analysis, $\boldsymbol{\theta}$ contains additional parameters, which are the coefficients of the time-dependent functions, e.g., $\mu(t)$, $\sigma(t)$, and $\xi(t)$

$$p(\boldsymbol{\theta}|Y, t) \propto \prod_{i=1}^{n} p(\boldsymbol{\theta}) \cdot p(y_i|\boldsymbol{\theta}, t) \tag{9}$$

In NEVA, the priors are noninformative normal distributions, for location and scale parameters, while the prior for the shape parameter is a normal distribution, with a standard deviation of 0.3, as suggested by Renard et al. (2013) and Cheng et al. (2014). The DE-MC algorithm is then implemented to sample a large number of realizations of θ over the parameter space (Cheng et al., 2014). The $\hat{R}$ criterion (Gelman & Shirley, 2011) is used to assess convergence, where $\hat{R}$ should remain below 1.1 (Cheng et al., 2014). Moreover, Bayes factor is implemented as a test for model selection: it compares the posterior distributions of two alternative models (e.g., stationary model versus nonstationary model) (Cheng et al., 2014; Renard et al., 2013). For further details about the Bayesian parameter estimation approach, the reader is referred to Cheng et al. (2014) and Cheng and AghaKouchak (2014).

In this study, the nonstationary GEV distribution refers to a GEV distribution with either the location parameter or location and scale parameters as a function of time. Hence, $\boldsymbol{\theta}$ is in the former case $\boldsymbol{\theta} = \{\mu_1, \mu_0, \sigma, \xi\}$, and in the latter $\boldsymbol{\theta} = \{\mu_1, \mu_0, \sigma_1, \sigma_0, \xi\}$. The selection of the nonstationary model versus a stationary model depends on the Mann-Kendall trend (MK, with 5% significance level) test, which characterizes the average behavior (mean) of the data over time. The mean can be regarded as an approximation of the location parameter of the GEV distribution. Hence, we modeled $\mu(t)$ to reproduce the observed trend. We assumed $\mu(t) = \mu_1 \cdot t + \mu_0$, because a more complex trend could likely result in an overfitting of the observation period and lead to an unrealistic representation of the future (Serinaldi & Kilsby, 2015). Even though more complex models are considered in the literature to be more accurate (e.g., Kwon & Lall, 2016; Sarhadi et al., 2016), parsimonious models (i.e., models showing desired level of performance efficiency with a minimum number of parameters) have shown to perform better (Luke et al., 2017; Serago & Vogel, 2017; Serinaldi & Kilsby, 2015). In the case of a time-dependent location parameter, the White test (White, 1980) for homoscedasticity is performed; if the null-hypothesis of constant variance in the residuals is rejected (with 5% significance level), we assumed a nonstationary model with time-dependent location and scale parameters. The scale parameter is modeled as $log(\sigma(t)) = \sigma_1 \cdot t + \sigma_0$, as suggested by Coles (2001) to ensure positivity. Finally, ξ was kept constant given the difficulties to precisely estimate it (Coles, 2001) especially for short time series (Papalexiou & Koutsoyiannis, 2013).

3.3. Incorporating Multimodel Simulations for IDF Curve Analysis

GCM projections can provide information on characteristics of future extremes. Consequently, we propose a new framework for deriving IDF curves of precipitation based on multimodel simulations. First, we derived the IDF curves for the climate models using the aforementioned Bayesian inference approach (i.e., NEVA). Since there is significant variability across the climate models (Figure 2), we chose to estimate the IDF curves for each model separately. We then merged the resulting IDF curves from each model to derive multimodel IDF curves. The final result is the expected IDF curve along with its uncertainty bounds, which summarize
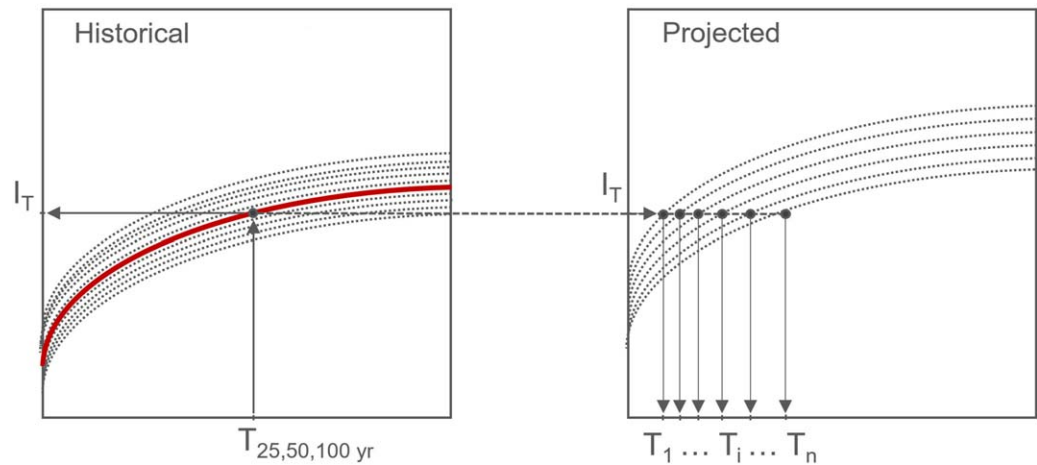
Figure 1. Conceptual explanation of the methodology adopted to quantify changes in the occurrences of historical events under future climate.

the variability due to both the parameter estimation approach (variability within each model) and the diversity of climatic models (variability across models).

Here we applied the proposed framework to annual precipitation maxima intensities from historical simulations $HE45^s_{m,d}$, and future climate $FE45^s_{m,d}$ and $FE85^s_{m,d}$. Consequently, for each station, we derived the historical multimodel IDF curves and future multimodel IDF curves based on RCP4.5 and RCP8.5 scenarios. We derived historical IDF curves imposing a stationary GEV model without performing a trend test to be consistent with NOAA's IDF curves. We then derived IDF curves from future climate projections RCP4.5 and RCP8.5 separately; the GEV model selected (stationary/nonstationary) depends upon the result of the Mann-Kendall trend test, and subsequent White test. GCMs provide gridded area average simulations while the current IDF curves available from NOAA are mainly based on point observations. Gridded area averaged observations are always smoother compared to point observations. Hence, we identified a bias by comparing historical IDF curves and NOAA IDF curves, which implies assuming a quantile-based bias. We then applied the same correction to historical and projected IDF curves.

In the case of a nonstationary GEV model, the GEV distribution function is time-dependent. The intensity of the p-event is then given by

$$q_p = \left(\left(-\frac{1}{\ln(p)} \right)^{\xi} - 1 \right) \cdot \frac{\hat{\sigma}}{\xi} + \hat{\mu} \tag{10}$$

where $\hat{\mu}$ is $\hat{\mu} = median(\mu(t))$ and $\hat{\sigma}$ is $\hat{\sigma} = median(\sigma(t))$. We selected $\hat{\mu}$ and $\hat{\sigma}$ within the period of the simulations to avoid any further projections of future climate.

Finally, we investigate how the frequency of past events is expected to change. Given the i'th set of GEV parameters (μ_i, σ_i, and ξ_i) from the ensemble of solution, the expected return period T_i is given by $\frac{1}{1-\Psi(I_T)}$, where $\Psi(I_T)$ is as follows:

$$\Psi(I_T) = \exp \left\{ - \left(1 + \xi_i \cdot \left(\frac{I_T - \mu_i}{\sigma_i} \right) \right)^{-\frac{1}{\xi_i}} \right\} \tag{11}$$

Consequently, a sample of the return periods T_i of an event of intensity I_T can be retrieved, Figure 1, and inference can be made.

In this study, we selected the intensity of a 1 day event with return period T, I_T, from the current NOAA precipitation frequency estimates for a specific location. To assess whether the recurrence of an event with intensity I_T is projected to change under future climate scenarios, we used the ensemble of return level curves retrieved via Bayesian inference to define IDF curves, and we derived the 0.25, 0.50, and 0.75 percentile of the ensemble. We then evaluated the expected future return period, along
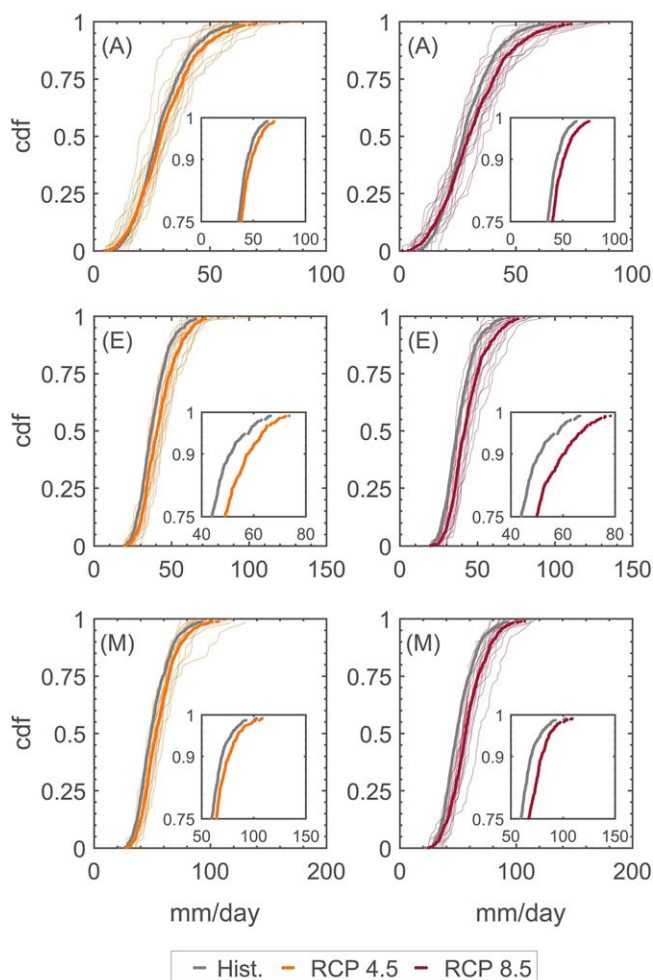
Figure 2. Comparison between 1 day extreme historical records (grey dotted line) and future climate (RPC4.5 orange and RCP8.5 red dotted line) ECDFs. The shaded dotted lines represent the uncertainty on the future climate. The inner boxes show the right tail behavior of the distributions. (A) San Diego (CA), (E) Chicago (IL), and (M) Atlanta (GA).

with its interquartile variability as the intersection between I_T and the 0.25, 0.50, and 0.75 percentile curves.

4. Results

The null-hypotheses of equal distributions ($\alpha = 1$) and equal means ($\alpha = 2$) between the median of historical records and the future climate projections are rejected ($p_{value} \sim 0$), indicating that the occurrence of future extreme precipitation intensities are likely to diverge from historical ones. This contradicts the commonly used stationary assumption in infrastructure design and risk assessment. Figure 2 shows the Empirical Cumulative Distribution Functions (ECDFs) of 1 day extreme precipitation for 3 of the selected stations; supporting information Table S2 summarizes the percent change in the median and in the 90th quantile of the simulated 1 day extreme precipitation intensity. The ECDFs of future climate precipitation extremes (Figure 2) display a shift toward the right, indicating that these cities may face an increase in severe rare events in the near future, even though there is high variability across the models. Overall, the RCP8.5 scenario seems to lead to more severe events. In the western US, the percent change in the median and the 90th quantile is around 10% for RCP4.5 and 10–15% RCP8.5. Sacramento (CA) and Salt Lake City (UT) are the exception, as they display a percent change around 20% for both scenarios (supporting information Table S2). In the eastern US, Chicago (IL), Nashville (TN), and New York (NY) display a 15–20% change in the median and 90th quantile for RCP8.5, while the remaining cities exhibit a change around 10% or below for both scenarios (supporting information Table S2).

IDF curves provide information on the magnitude and recurrence of extreme events based on frequency analysis. For this reason, shifts in extreme rainfall distribution will affect how the IDF curves are defined, and will also affect the intensity of the design value for the event. Therefore, the resilience of infrastructures and natural and engineered slopes can be compromised. Figures 3–5 show pairs of current and projected IDF curves along with the 90% confidence interval (or Credible Interval) within and across climatic models based on RCP8.5 scenario (see supporting information Figures S1–S3 for RCP4.5) Under the future scenarios chosen, our results show an overall upward shift of the IDF curves, indicating that more severe events are expected to occur. Assuming that climate model simulations provide reasonable estimates of future extremes, Figure 6b and supporting information Figure S4 show the so-called safety factors C (i.e., ratio of medians of the future relative to the past IDF curves), if one is interested in adjusting current design values to cope with a changing climate. In western US, the intensity of extreme events could potentially experience a 20% increase, e.g., Salt Lake City and Sacramento (Figure 6b).

After investigating the change in extreme event intensity for a fixed return period, we explored changes in the frequency of extreme events of 1 day duration for a given event magnitude. Specifically, we chose the intensity of three baseline events corresponding to 25, 50, and 100 year events (retrieved from current NOAA IDF curves) to estimate their expected occurrence in the future, along with their interquartile range (IQR). Figure 6a shows the return periods expected in the future of the baseline events (dots), along with the IQR (gray lines). Events expected to occur every 50 or 100 years are becoming more frequent, raising public safety concerns within anthropized environments, especially in the western US. For example, climate model simulations project that the frequency of a 50 year event in the future will double in San Diego (CA) and Salt Lake City (UT).
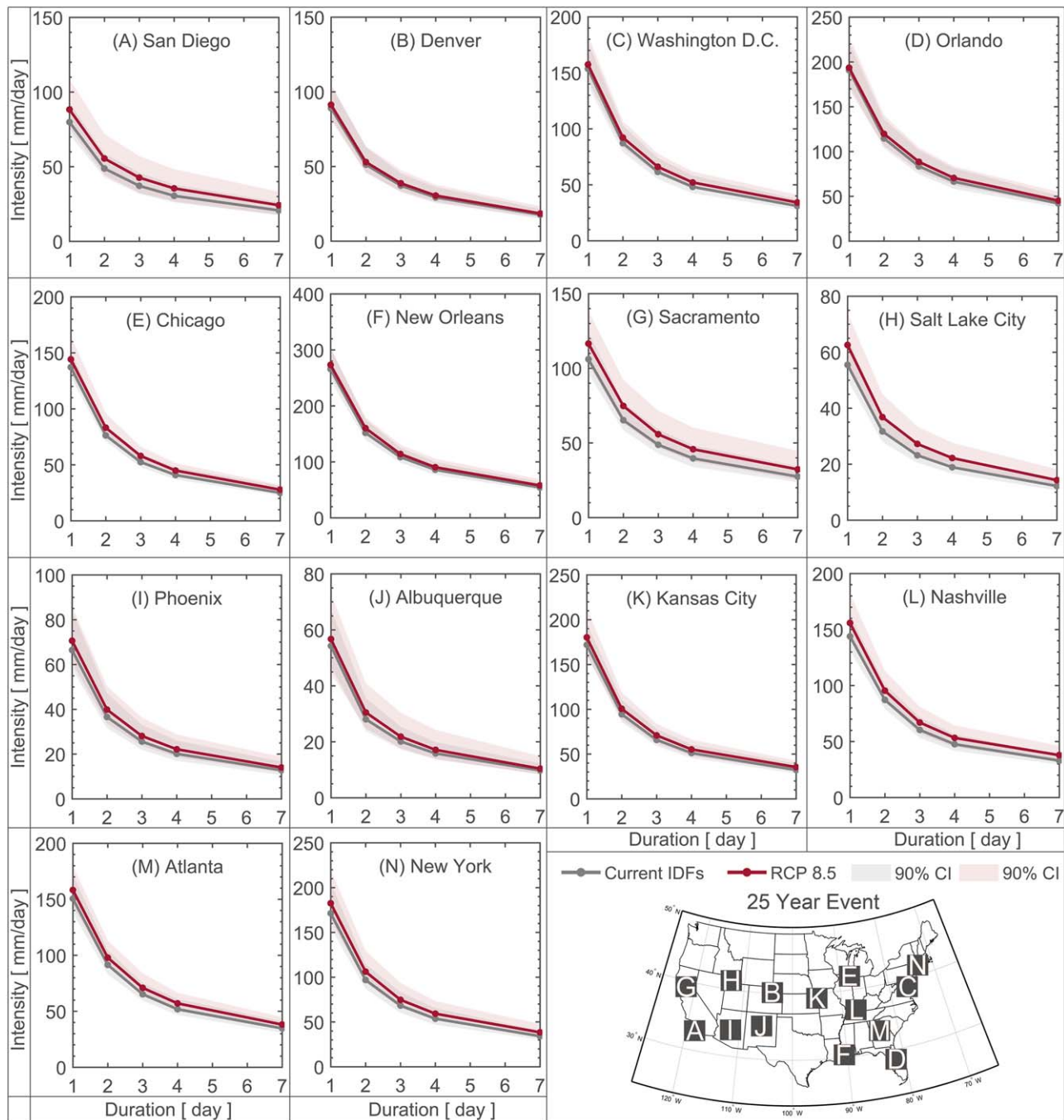
Figure 3. RCP8.5—comparison between current (grey lines) and future climate scenario (red lines) IDF curves, along with 90% confidence intervals, given an average return interval of 25 years.

Although the future scenarios predict changes in magnitude and frequency of extreme precipitation events, total annual mean rainfall is expected to remain the same. Figure 6c shows that locations in the eastern US register an increase in mean total annual precipitation and moderate changes in extreme events, whereas locations in the western US do not expect to receive more water overall than in the past, even though extreme events are predicted to become more severe and more likely. A recent study argues that drought conditions in California, linked to warmer temperatures, have been worsened over the past decades, even though negative precipitation anomalies have not shown any change (Diffenbaugh et al., 2015). Analogously, in California, we observed total annual precipitation in a future climate consistent with the past.
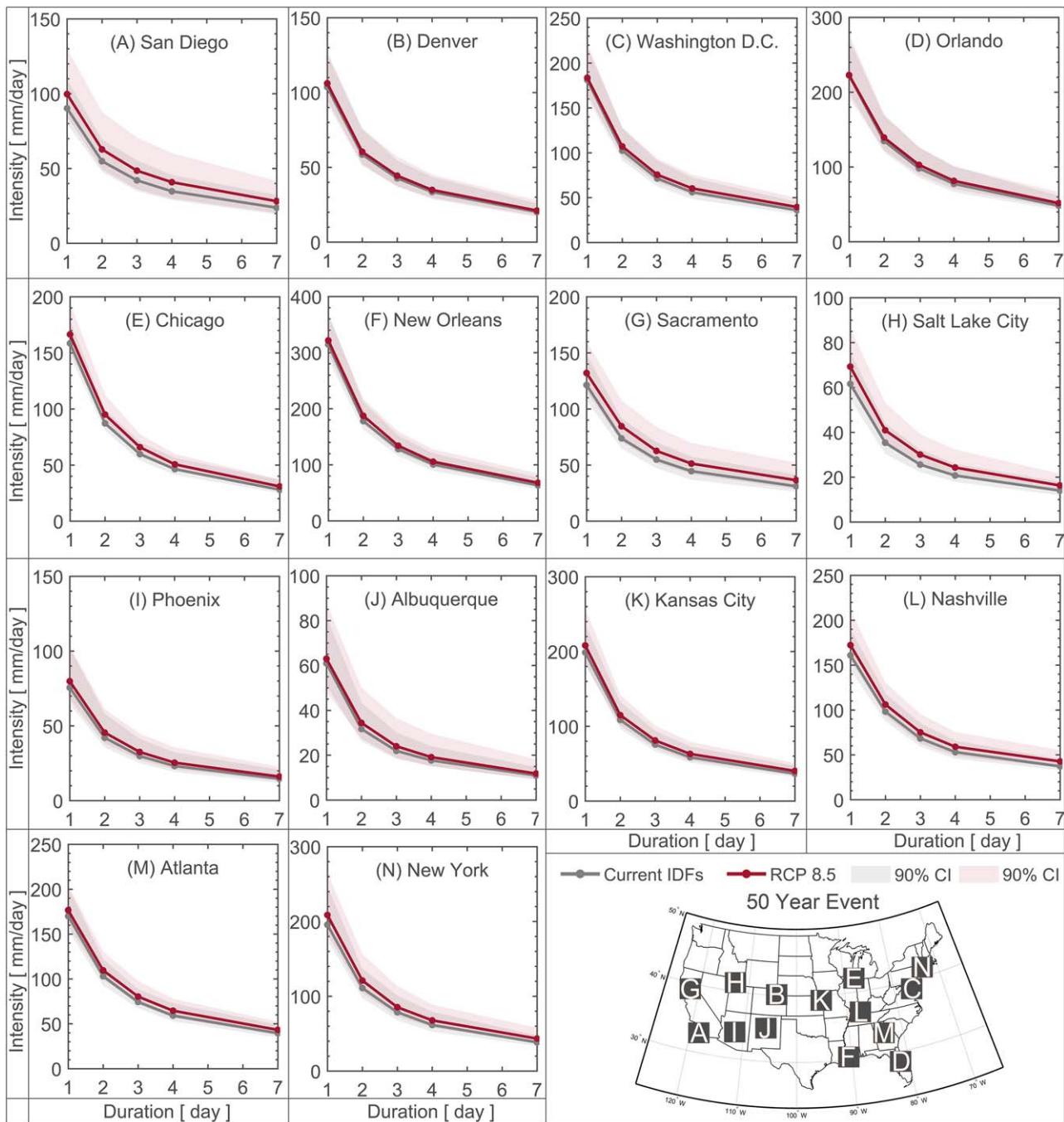
Figure 4. RCP8.5—comparison between current (grey lines) and future climate scenario (red lines) IDF curves, along with 90% confidence intervals, given an average return interval of 50 years.

Consequently, to better characterize meteorological extremes over the state, we analyzed a number of urban locations mainly along California's coast (supporting information Table S3), adopting the same procedures used for the other urban stations across the United States. California's IDF curves are shown in supporting information Figures S10–S15. However, we only used the four GCMs as recommended by the guidelines for originating the California's Fourth Climate Change Assessment Report (supporting information Table S4) that offer much higher spatial resolution (1/16°). Our results suggest a substantial increase in the severity of future extreme precipitation events for RCP8.5 scenario (Figure 7). The results indicate an
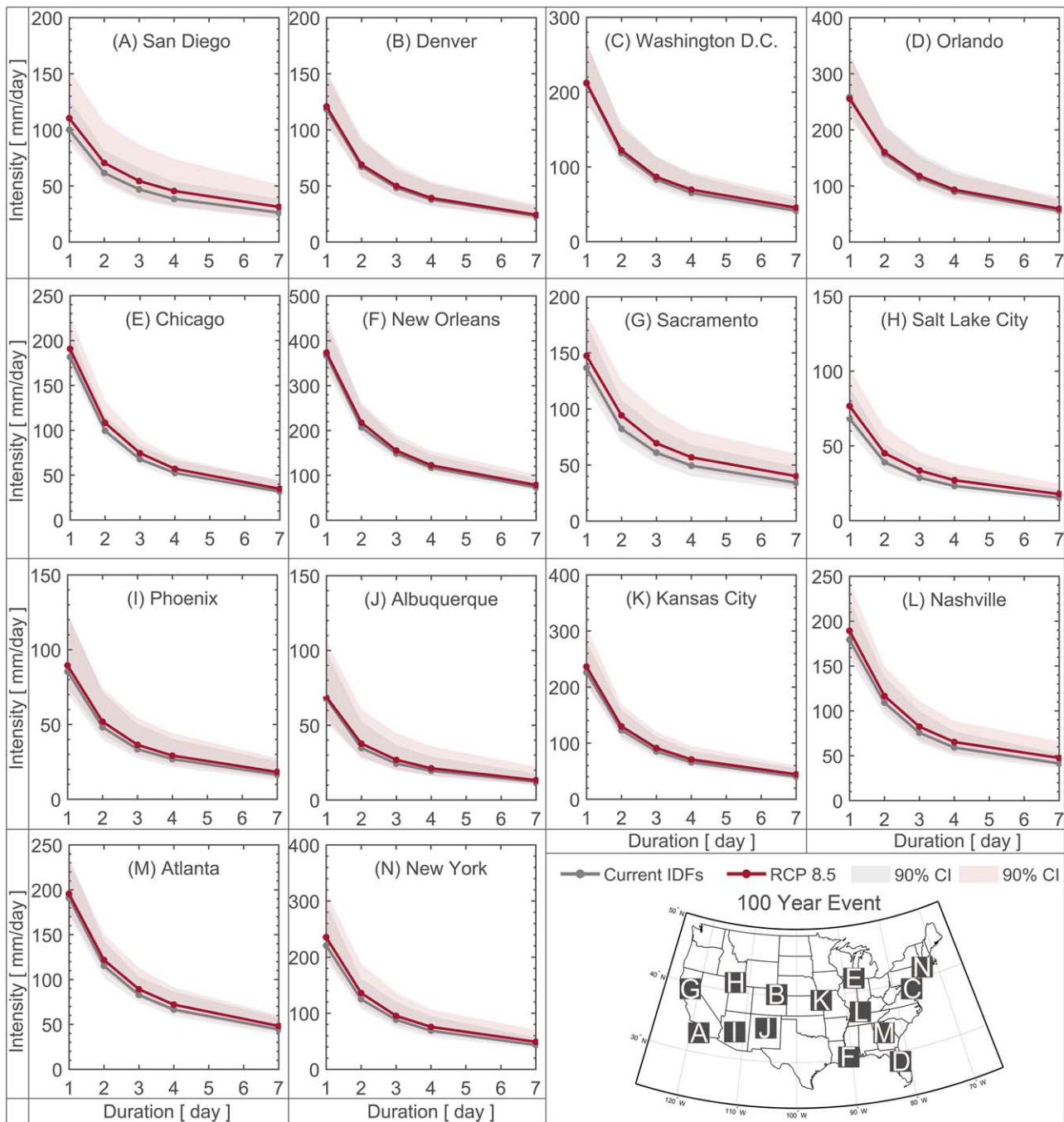
Figure 5. RCP8.5—comparison between current (grey lines) and future climate scenario (red lines) IDF curves, along with 90% confidence intervals, given an average return interval of 100 years.

approximately threefold increase in occurrences of extremes relative to past events, particularly in southern California (Figure 7).

5. Conclusion and Discussion

In this study, we have shown the potential impacts of a warming climate on extreme precipitation intensity and recurrence interval. Urban areas, especially in the western US, may struggle against increases in severity and frequency of rare events. Increase in intensity, duration, and frequency of extreme precipitation can
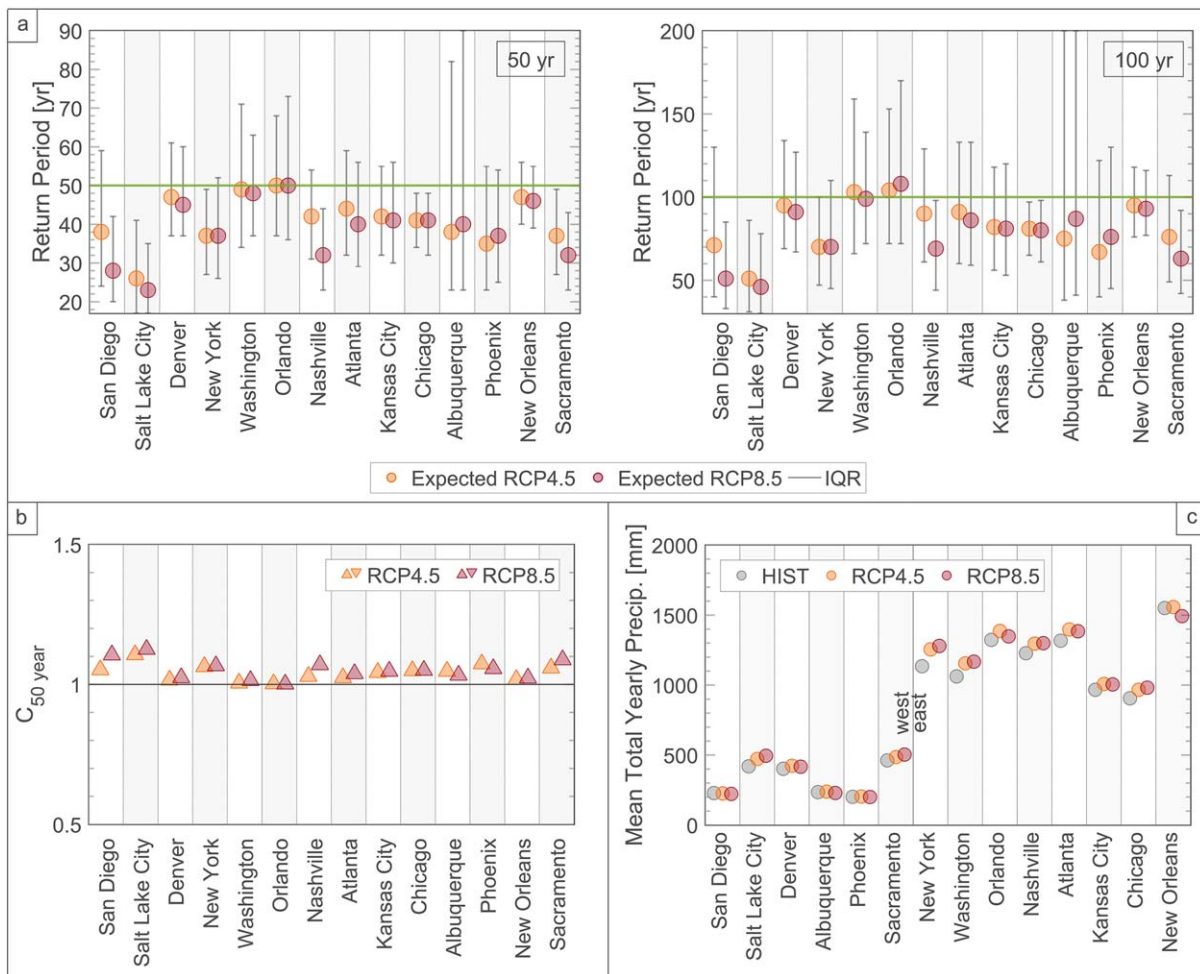
Figure 6. (a) Return periods under future climate of events currently associated with return periods of 50 and 100 years in urban locations across the United States: expected projected return periods (dots) along with interquartile range (IQR—grey lines). (b) Safety factors (i.e., ratio of medians of the future relative to the past IDF curves). (c) Total annual mean precipitation of historical records.
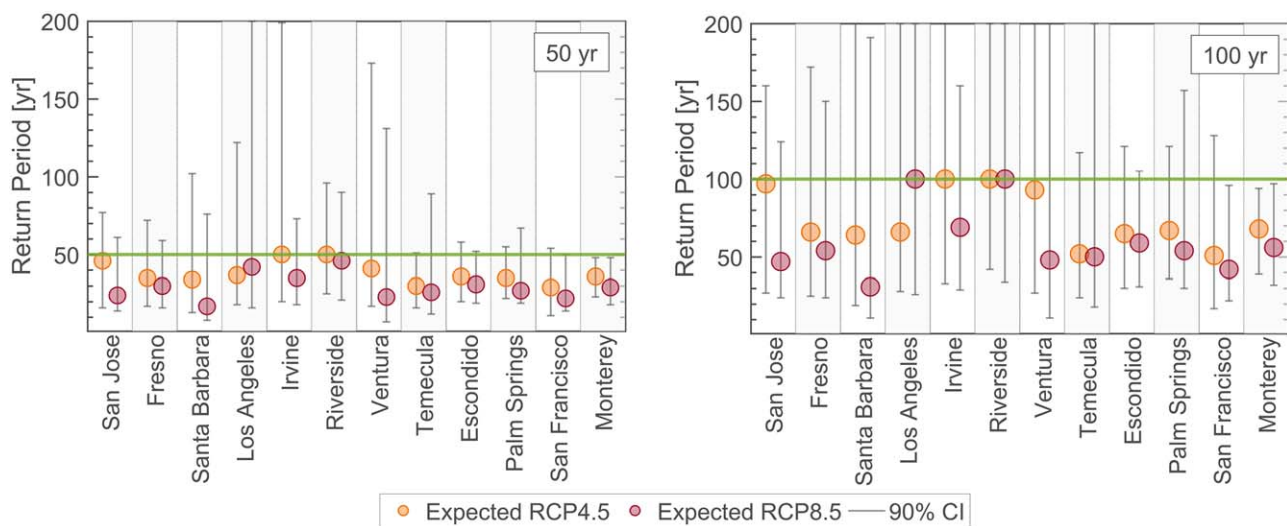
Figure 7. Return periods under future climate of events historically associated with return periods of 50 and 100 years in California. Expected projected return periods (dots) and 90% confidence interval (gray lines).

adversely impact the integrity of infrastructure and natural and engineered slopes. Infrastructure built with soil (e.g., earthen dams, levees, and embankments), or that interface with soil (e.g., roads, bridge, pipelines, and foundations), are more vulnerable because severe rainfall causes soil erosion and, upon infiltration, can significantly reduce the strength of soil. The topic of infrastructure resilience is even more important in regions where multiple drivers of change coincide. Coastal cities, for example, are even more vulnerable due to the compounding effects of sea level rise and change in climate (Hallegatte et al., 2013). By 2070, the population jeopardized by extreme floods is expected to increase threefold with exposed assets increasing by approximately 9% of the projected global GPD of the same period (Hanson et al., 2011).

We argue that better infrastructure planning and maintenance is fundamental for a resilient society. The proposed method for addressing nonstationarity in future climate scenarios can reduce the risk of underestimating future extreme precipitation events and their severity. The adaptation of existing infrastructure, which were designed assuming a stationary climate, requires assessing their performance under future climate scenarios. Further, it requires revisiting design guidelines for infrastructure to employ nonstationary IDF curves in future design procedures.

References

Anderson, T. W. (1962). On the distribution of the two-sample Cramer-von Mises criterion. *The Annals of Mathematical Statistics*, *33*(3), 1148–1159. https://doi.org/10.1214/aoms/1177704477

Anderson, T. W. (2011). *Anderson-Darling tests of goodness-of-fit* (pp. 52–54). Berlin, Heidelberg: Springer.

Barnett, T. P., Hasselmann, K., Chelliah, M., Delworth, T., Hegerl, G., Jones, P., et al. (1999). Detection and attribution of recent climate change: A status report. *Bulletin of the American Meteorological Society*, *80*(12), 2631–2659. https://doi.org/10.1175/1520-0477(1999)080<2631:DAAORC>2.0.CO;2

Bonnin, G., Perica, S., Dietz, S., Heim, S., Hiner, L., Maitaria, K., et al. (2006). Precipitation-frequency atlas of the united states, *NOAA Atlas*, *14*, 1–10.

Brekke, L., Thrasher, B., Maurer, E., & Pruitt, T. (2013). *Downscaled cmip3 and cmip5 climate and hydrology projections: Release of downscaled cmip5 climate projections, comparison with preceding information, and summary of user needs*. Denver, CO: US Department of the Interior, Bureau of Reclamation, Technical Services Center.

Cheng, L., & AghaKouchak, A. (2014). Nonstationary precipitation intensity-duration-frequency curves for infrastructure design in a changing climate. *Scientific Reports*, *4*, 7093.

Cheng, L., AghaKouchak, A., Gilleland, E., & Katz, R. W. (2014). Non-stationary extreme value analysis in a changing climate. *Climatic Change*, *127*(2), 353–369. https://doi.org/10.1007/s10584-014-1254-5

Cohn, T. A., & Lins, H. F. (2005). Nature's style: Naturally trendy. *Geophysical Research Letters*, *32*, L23402. https://doi.org/10.1029/2005GL024476

Coles, S. (2001). *An introduction to statistical modeling of extreme values*. London, UK: Springer.

Cooley, D., Nychka, D., & Naveau, P. (2007). Bayesian spatial modeling of extreme precipitation return levels. *Journal of the American Statistical Association*, *102*(479), 824–840. https://doi.org/10.1198/016214506000000780

DeGaetano, A. T. (2009). Time-dependent changes in extreme-precipitation return-period amounts in the Continental United States. *Journal of Applied Meteorology and Climatology*, *48*(10), 2086–2099. https://doi.org/10.1175/2009JAMC2179.1

Diffenbaugh, N. S., Swain, D. L., & Touma, D. (2015). Anthropogenic warming has increased drought risk in California. *Proceedings of the National Academy of Sciences of the United States of America*, *112*(13), 3931–3936.

Fischer, E. M., & Knutti, R. (2015). Anthropogenic contribution to global occurrence of heavy-precipitation and high-temperature extremes. *Nature Climate Change*, *5*(6), 560–564.

Fischer, E. M., & Knutti, R. (2016). Observed heavy precipitation increase confirms theory and early models. *Nature Climate Change*, *6*, 986–991. https://doi.org/https://doi.org/10.1038/nclimate3110

Gariano, S. L., & Guzzetti, F. (2016). Landslides in a changing climate. *Earth-Science Reviews*, *162*, 227–252. https://doi.org/10.1016/j.earscirev.2016.08.011

Gelman, A., & Shirley, K. (2011). Inference from simulation and monitoring convergence. In Brooks, S., Gelman, A., Jones, G. L., & Meng, X.-L. (Eds.), *Handbook of Markov Chain Monte Carlo* (Chapter 6, pp. 163–174). London, UK: Chapman & Hall/CRC.

Hallegatte, S., Green, C., Nicholls, R. J., & Corfee-Morlot, J. (2013). Future flood losses in major coastal cities. *Nature Climate Change*, *3*(9), 802–806.

Hanson, S., Nicholls, R., Ranger, N., Hallegatte, S., Corfee-Morlot, J., Herweijer, C., et al. (2011). A global ranking of port cities with high exposure to climate extremes. *Climatic Change*, *104*(1), 89–111. https://doi.org/10.1007/s10584-010-9977-4

Hidalgo, H. G., Dettinger, M. D., & Cayan, D. R. (2008). Downscaling with constructed analogues: Daily precipitation and temperature fields over the United States (Technical report Series Number 2007-027). California Energy Commission, PIER Energy Related Environmental Research.

Huard, D., Mailhot, A., & Duchesne, S. (2009). Bayesian estimation of Intensity-Duration-Frequency curves and of the return period associated to a given rainfall event. *Stochastic Environmental Research and Risk Assessment*, *24*(3), 337–347. https://doi.org/10.1007/s00477-009-0323-1

Jasim, F. H., Vahedifard, F., Ragno, E., AghaKouchak, A., & Ellithy, G. (2017). Effects of climate change on fragility curves of earthen levees subjected to extreme precipitations. In *Geo-Risk 2017: Geotechnical risk from theory to practice* (Geotechnical Special Publication No. 285, pp. 498–507). Denver, CO, Reston, VA: American Society of Civil Engineers (ASCE). https://doi.org/10.1061/9780784480724.045

Katz, R. W. (2013). Statistical methods for nonstationary extremes. In AghaKouchak, A., Easterling, D., Hsu, K., Schubert, S., & Sorooshian, S. (Eds.), *Extremes in a changing climate: Detection, analysis and uncertainty* (pp. 15–37). Netherlands, Dordrecht: Springer. https://doi.org/10.1007/978-94-007-4479-0_2

Katz, R. W., Parlange, M. B., & Naveau, P. (2002). Statistics of extremes in hydrology. *Advances in Water Resources*, *25*(8–12), 1287–1304. https://doi.org/10.1016/S0309-1708(02)00056-8

Koutsoyiannis, D. (2005). Nonstationarity versus scaling in hydrology. *Journal of Hydrology*, *324*(1–4), 239–254. https://doi.org/10.1016/j.jhydrol.2005.09.022

Koutsoyiannis, D., & Montanari, A. (2015). Negligent killing of scientific concepts: The stationarity case. *Hydrological Sciences Journal*, *60*(7–8), 1174–1183. https://doi.org/10.1080/02626667.2014.959959

Krishnaswamy, J., Vaidyanathan, S., Rajagopalan, B., Bonell, M., Sankaran, M., Bhalla, R. S., et al. (2015). Non-stationary and non-linear influence of Enso and Indian Ocean dipole on the variability of Indian monsoon rainfall and extreme rain events. *Climate Dynamics*, *45*(1), 175–184. https://doi.org/10.1007/s00382-014-2288-0

Kwon, H. H., & Lall, U. (2016). A copula-based nonstationary frequency analysis for the 2012–2015 drought in California. *Water Resources Research*, *52*, 5662–5675. https://doi.org/10.1002/2016WR018959

Lima, C. H., Kwon, H.-H., & Kim, J.-Y. (2016). A Bayesian beta distribution model for estimating rainfall IDF curves in a changing climate. *Journal of Hydrology*, *540*, 744–756. https://doi.org/10.1016/j.jhydrol.2016.06.062

Lins, H. F., & Cohn, T. A. (2011). Stationarity: Wanted dead or alive? *Journal of the American Water Resources Association*, *47*(3), 475–480. https://doi.org/10.1111/j.1752-1688.2011.00542.x

Luke, A., Vrugt, J., AghaKouchak, A., Matthew, R., & Sanders, B. (2017). Modeling and mitigating natural hazards: Stationarity is immortal! *Water Resources Research*, *50*, 9748–9756. https://doi.org/10.1002/2014WR016092

Mailhot, A., & Duchesne, S. (2010). Design criteria of urban drainage infrastructures under climate change. *Journal of Water Resources Planning and Management*, *136*(2), 201–208. https://doi.org/10.1061/(ASCE)WR.1943-5452.0000023

Mailhot, A., Duchesne, S., Caya, D., & Talbot, G. (2007). Assessment of future change in intensity-duration-frequency (IDF) curves for Southern Quebec using the Canadian Regional Climate Model (CRCM). *Journal of Hydrology*, *347*(12), 197–210. https://doi.org/10.1016/j.jhydrol.2007.09.019

Mann, H. B. (1945). Nonparametric tests against trend. *Econometrica*, *13*(3), 245–259.

Marvel, K., & Bonfils, C. (2013). Identifying external influences on global precipitation. *Proceedings of the National Academy of Sciences of the United States of America*, *110*(48), 19301–19306. https://doi.org/10.1073/pnas.1314382110

Massey, F. J. (1951). The Kolmogorov-Smirnov test for goodness of fit. *Journal of the American Statistical Association*, *46*(253), 68–78.

Mazdiyasni, O., & AghaKouchak, A. (2015). Substantial increase in concurrent droughts and heatwaves in the United States. *Proceedings of the National Academy of Sciences of the United States of America*, *112*(37), 11484–11489.

Melillo, J. M., Terese, T. C. R., & Yohe, G. W., (Eds.). (2014). Highlights of climate change impacts in the United States: The third national climate assessment (148 pp.). U.S. Global Change Research Program.

Milly, P. C. D., Betancourt, J., Falkenmark, M., Hirsch, R. M., Kundzewicz, Z. W., Lettenmaier, D. P., et al. (2008). Stationarity is dead: Whither water management? *Science*, *319*(5863), 573–574. https://doi.org/10.1126/science.1151915

Min, S.-K., Zhang, X., Zwiers, F. W., & Hegerl, G. C. (2011). Human contribution to more-intense precipitation extremes. *Nature*, *420*, 378–381. https://doi.org/https://doi.org/10.1038/nature09763

Mirhosseini, G., Srivastava, P., & Fang, X. (2014). Developing rainfall intensity-duration-frequency curves for Alabama under future climate scenarios using artificial neural networks. *Journal of Hydrologic Engineering*, *19*(11), 04014022-1–04014022-10. https://doi.org/10.1061/(ASCE)HE.1943-5584.0000962

Mirhosseini, G., Srivastava, P., & Sharifi, A. (2015). Developing probability-based IDF curves using kernel density estimator. *Journal of Hydrologic Engineering*, *20*(9), 04015002-1–04015002-11. https://doi.org/10.1061/(ASCE)HE.1943-5584.0001160

Moftakhari, H. R., Salvadori, G., AghaKouchak, A., Sanders, B. F., & Matthew, R. A. (2017). Compounding effects of sea level rise and fluvial flooding. *Proceedings of the National Academy of Sciences of the United States of America*, *114*(37), 9785–9790. https://doi.org/10.1073/pnas.1620325114

Mondal, A., & Mujumdar, P. (2015). Modeling non-stationarity in intensity, duration and frequency of extreme rainfall over India. *Journal of Hydrology*, *521*, 217–231.

Montanari, A., & Koutsoyiannis, D. (2014). Modeling and mitigating natural hazards: Stationary is immortal! *Water Resources Research*, *50*, 9748–9756. https://doi.org/10.1002/2014WR016092

Obeysekera, J., & Salas, J. D. (2013). Quantifying the uncertainty of design floods under nonstationary conditions. *Journal of Hydrologic Engineering*, *19*(7), 1438–1446.

Pachauri, R. K., Allen, M. R., Barros, V. R., Broome, J., Cramer, W., Christ, R., et al. (2014). *Climate change 2014: Synthesis report. Contribution of Working Groups I, II and III to the fifth assessment report of the Intergovernmental Panel on Climate Change*. Geneva, Switzerland: Intergovernmental Panel on Climate Change.

Papalexiou, S. M., & Koutsoyiannis, D. (2013). Battle of extreme value distributions: A global survey on extreme daily rainfall. *Water Resources Research*, *49*, 187–201. https://doi.org/10.1029/2012WR012557

Read, L. K., & Vogel, R. M. (2015). Reliability, return periods, and risk under nonstationarity. *Water Resources Research*, *51*, 6381–6398. https://doi.org/10.1002/2015WR017089

Renard, B., Sun, X., & Lang, M. (2013). Extremes in a changing climate: Detection, analysis and uncertainty. In AghaKouchak, A., Easterling, D., Hsu, K., Schubert, S., & Sorooshian, S. (Eds.), *Bayesian methods for non-stationary extreme value analysis* (pp. 39–95). Dordrecht, Netherlands: Springer.

Rizzo, M. L., & Székely, G. J. (2010). Disco analysis: A nonparametric extension of analysis of variance. *Annals of Applied Statistics*, *4*(2), 1034–1055. https://doi.org/10.1214/09-AOAS245

Robinson, J. D., Vahedifard, F., & AghaKouchak, A. (2017). Rainfall-triggered slope instabilities under a changing climate: Comparative study using historical and projected precipitation extremes. *Canadian Geotechnical Journal*, *54*(1), 117–127. https://doi.org/10.1139/cgj-2015-0602

Rosner, A., Vogel, R. M., & Kirshen, P. H. (2014). A risk-based approach to flood management decisions in a nonstationary world. *Water Resources Research*, *50*, 1928–1942. https://doi.org/10.1002/2013WR014561

Sadegh, M., Vrugt, J. A., Xu, C., & Volpi, E. (2015). The stationarity paradigm revisited: Hypothesis testing using diagnostics, summary metrics, and dream(abc). *Water Resources Research*, *51*, 9207–9231. https://doi.org/10.1002/2014WR016805

Salas, J. D., & Obeysekera, J. (2013). Revisiting the concepts of return period and risk for nonstationary hydrologic extreme events. *Journal of Hydrologic Engineering*, *19*(3), 554–568.

Sankarasubramanian, A., & Lall, U. (2003). Flood quantiles in a changing climate: Seasonal forecasts and causal relations. *Water Resources Research*, *39*(5), 1134. https://doi.org/10.1029/2002WR001593

Sarhadi, A., Burn, D. H., Concepción Ausín, M., & Wiper, M. P. (2016). Time-varying nonstationary multivariate risk analysis using a dynamic Bayesian copula. *Water Resources Research*, *52*, 2327–2349. https://doi.org/10.1002/2015WR018525

Sarhadi, A., & Soulis, E. D. (2017). Time-varying extreme rainfall intensity-duration-frequency curves in a changing climate. *Geophysical Research Letters*, *44*, 2454–2463. https://doi.org/10.1002/2016GL072201

Serago, J. M., & Vogel, R. M. (2017). Parsimonious nonstationary flood frequency analysis. *Advances in Water Resources*, *112*, 1–16. https://doi.org/10.1016/j.advwatres.2017.11.026

Serinaldi, F., & Kilsby, C. G. (2015). Stationarity is undead: Uncertainty dominates the distribution of extremes. *Advances in Water Resources*, *77*, 17–36. https://doi.org/10.1016/j.advwatres.2014.12.013

Stott, P. A., Gillett, N. P., Hegerl, G. C., Karoly, D. J., Stone, D. A., Zhang, X., et al. (2010). Detection and attribution of climate change: A regional perspective. *Wiley Interdisciplinary Reviews: Climate Change*, *1*(2), 192–211. https://doi.org/10.1002/wcc.34

Székely, G. J., & Rizzo, M. L. (2013). Energy statistics: A class of statistics based on distances. *Journal of Statistical Planning and Inference*, *143*(8), 1249–1272.

Vahedifard, F., Tehrani, F. S., Galavi, V., Ragno, E., & AghaKouchak, A. (2017). Resilience of MSE walls with marginal backfill under a changing climate: Quantitative assessment for extreme precipitation events. *Journal of Geotechnical and Geoenvironmental Engineering*, *143*(9), 04017056-1–04017056-14. https://doi.org/10.1061/(ASCE)GT.1943-5606.0001743

Villarini, G., Smith, J. A., & Napolitano, F. (2010). Nonstationary modeling of a long record of rainfall and temperature over Rome. *Advances in Water Resources*, *33*(10), 1256–1267. https://doi.org/10.1016/j.advwatres.2010.03.013

Villarini, G., Smith, J. A., Serinaldi, F., Bales, J., Bates, P. D., & Krajewski, W. F. (2009). Flood frequency analysis for nonstationary annual peak records in an urban drainage basin. *Advances in Water Resources*, *32*(8), 1255–1266. https://doi.org/10.1016/j.advwatres.2009.05.003

Vogel, R. M., Yaindl, C., & Walter, M. (2011). Nonstationarity: Flood magnification and recurrence reduction factors in the united states1. *JAWRA Journal of the American Water Resources Association*, *47*(3), 464–474. https://doi.org/10.1111/j.1752-1688.2011.00541.x

Volpi, E., Fiori, A., Grimaldi, S., Lombardo, F., & Koutsoyiannis, D. (2015). One hundred years of return period: Strengths and limitations. *Water Resources Research*, *51*, 8570–8585. https://doi.org/10.1002/2015WR017820

Wasko, C., Sharma, A., & Westra, S. (2016). Reduced spatial extent of extreme storms at higher temperatures. *Geophysical Research Letters*, *43*, 4026–4032. https://doi.org/10.1002/2016GL068509

Westra, S., Alexander, L. V., & Zwiers, F. W. (2013). Global increasing trends in annual maximum daily precipitation. *Journal of Climate*, *26*(11), 3904–3918. https://doi.org/10.1175/JCLI-D-12-00502.1

White, H. (1980). A heteroskedasticity-consistent covariance matrix estimator and a direct test for heteroskedasticity. *Econometrica*, *48*(4), 817–838.

Willems, P., Arnbjerg-Nielsen, K., Olsson, J., & Nguyen, V. (2012). Climate change impact assessment on urban rainfall extremes and urban drainage: Methods and shortcomings. *Atmospheric Research*, *103*, 106–118. https://doi.org/10.1016/j.atmosres.2011.04.003

Yan, H., Sun, N., Wigmosta, M., Skaggs, R., Hou, Z., & Leung, R. (2018). Next-generation intensity-duration-frequency curves for hydrologic design in snow-dominated environments. *Water Resources Research*, *54*. https://doi.org/10.1002/2017WR021290

Yilmaz, A. G., & Perera, B. J. C. (2014). Extreme rainfall nonstationarity investigation and intensity-frequency-duration relationship. *Journal of Hydrologic Engineering*, *19*(6), 1160–1172. https://doi.org/10.1061/(ASCE)HE.1943-5584.0000878

Zhang, X., Zwiers, F. W., Hegerl, G. C., Lambert, F. H., Gillett, N. P., Solomon, S., et al. (2007). Detection of human influence on twentieth-century precipitation trends. *Nature*, *448*(7152), 461–465.

Zhang, X., Zwiers, F. W., & Stott, P. A. (2006). Multimodel multisignal climate change detection at regional scale. *Journal of Climate*, *19*(17), 4294–4307. https://doi.org/10.1175/JCLI3851.1

Zheng, F., Westra, S., & Michael, L. (2105). Opposing local precipitation extremes. *Nature Climate Change*, *5*, 389–390. https://doi.org/https://doi.org/10.1038/nclimate2579

Zhu, J., Stone, M. C., & Forsee, W. (2012). Analysis of potential impacts of climate change on Intensity-Duration-Frequency (IDF) relationships for six regions in the United States. *Journal of Water and Climate Change*, *3*, 185–196. https://doi.org/10.2166/wcc.2012.045

Zwiers, F. W., Zhang, X., & Feng, Y. (2011). Anthropogenic influence on long return period daily temperature extremes at regional scales. *Journal of Climate*, *24*(3), 881–892. https://doi.org/10.1175/2010JCLI3908.1